

Magnetised Neutron Star Crusts and Torsional Shear Modes of Magnetars

Rana Nandi and Debades Bandyopadhyay

Astroparticle Physics and Cosmology Division, Saha Institute of Nuclear Physics, 1/AF
Bidhannagar, Kolkata-700064, India

E-mail: debades.bandyopadhyay@saha.ac.in

Abstract. We discuss outer and inner crusts of neutron stars in strong magnetic fields. Here, we demonstrate the effect of Landau quantization of electrons on the ground state properties of matter in outer and inner crusts in magnetars. This effect leads to the enhancement of the electron number density in strong magnetic fields with respect to the zero field case. For the outer crust, we adopt the magnetic Baym-Pethick-Sutherland model and obtain the sequence of nuclei and equation of state (EoS). The properties of nuclei in the inner crust in the presence of strong magnetic fields are investigated using the Thomas-Fermi model. The coexistence of two phases of nuclear matter - liquid and gas, is assumed in this case. The proton number density in the Wigner-Seitz cell is affected in strong magnetic fields through the charge neutrality. We perform this calculation using the Skyrme nucleon-nucleon interaction with different parameterisations. We find nuclei with larger mass and atomic numbers in the inner crust in the presence of strong magnetic fields than those of the zero field case for all those parameter sets. Further we investigate torsional shear mode frequencies using the results of magnetised neutron star crusts and compare those with observations.

1. Introduction

Neutron star crust plays an important role in many observational findings on neutron stars [1]. Heat transport and magnetic field evolution in the crust are sensitive to the composition of the crust. This, in turn, might influence various transport properties such as electrical and thermal conductivities, shear modulus and shear viscosity in the neutron star crust. Figure 1 demonstrates different regions of a neutron star schematically. The crustal region is just beneath the envelope as shown in the figure. Neutron star crust is separated into outer and inner crust. The outer crust begins at $\sim 10^4 g/cm^3$. The thickness of the outer crust is a few hundred meters. The outer crust is made of nuclei arranged in a body-centered cubic (bcc) lattice and embedded in a uniform background of electrons which become relativistic at a density $\sim 10^7 g/cm^3$. Neutrons and protons are bound in nuclei in this case. The equilibrium nucleus at $\sim 10^4 g/cm^3$ is ^{56}Fe . Equilibrium nuclei become more and more neutron rich as density increases. The neutron chemical potential exceeds the neutron rest mass at a density $\sim 4 \times 10^{11} g/cm^3$. Consequently, neutrons drip out of nuclei and it is called the neutron drip point. This is the end of the outer crust and the beginning of the inner crust. The inner crust is composed of neutron rich nuclei arranged in a bcc lattice and also in coexistence with dripped neutrons and a uniform background of electrons. The thickness of the inner crust is ~ 1 km. More and more neutrons come out of neutron rich nuclei with increasing density. Finally, nuclei of the inner

crust dissolve into a uniform nuclear matter at the crust-core boundary.

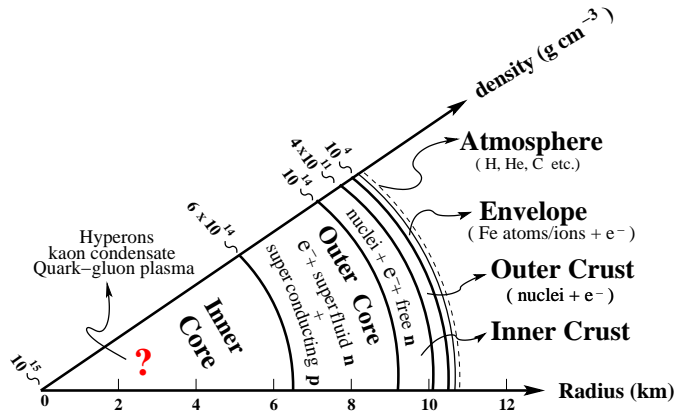


Figure 1. Schematic structure of a neutron star interior.

Extreme physical condition such as very strong surface magnetic fields $\sim 10^{15}$ G were found to exist in a class of neutron stars called magnetars [2, 3]. Even stronger interior field could exist in magnetars. Magnetars are classified into two groups - Anomalous x-ray pulsars (AXPs) and soft gamma-ray repeaters (SGRs) [4, 5]. SGRs are found to emit sporadic bursts of soft gamma rays. It was observed that SGRs occasionally emit stronger gamma rays known as giant flares having luminosities as high as 10^{46} ergs s^{-1} [6, 7, 8, 9]. Giant flares are considered to be the result of evolving magnetic field and its stress on the magnetar crust. In the decaying tail of giant flares, quasi-periodic oscillations (QPOs) were observed over long duration [7, 8, 9]. QPOs were identified as torsional shear modes of magnetar crust [3]. The study of QPOs might shed light on the ground state properties of magnetar crust.

Recent studies showed that high magnetic fields associated with magnetars would influence the composition and EoS of neutron star crusts which, in turn, might have impact on the QPO frequencies. In this paper, we study and discuss this problem. The paper is organised in the following way. We discuss the composition and EoS of neutron star crusts with or without magnetic field in section 2. Torsional shear modes are discussed in section 3. We summarise in section 4.

2. Composition and EoS of Neutron Star Crust

In a seminal paper, Baym, Pethick and Sutherland (BPS) studied the equilibrium composition and EoS of the ground state matter of the outer crust without magnetic field [10]. Later this BPS model was extended to include the effects of strong magnetic fields [11]. High magnetic fields of magnetars might influence the composition and EoS through Landau quantisation. Recently we have revisited the magnetic BPS model. Furthermore, we include the finite size effect in the lattice energy and adopted recent experimental and theoretical mass tables [12]. We adopt the Wigner-Seitz approximation in this calculation. The equilibrium sequence of nuclei is determined by minimising the Gibbs free energy per baryon (g) with respect to mass number (A) and atomic number (Z) at a constant pressure (P) [10],

$$\begin{aligned}
 g &= \frac{E_{tot} + P}{n_b} = \frac{W_N + 4/3W_L + Z\mu_e}{A}, \\
 E_{tot} &= n_N(W_N + W_L) + \varepsilon_e(n_e), \\
 P &= P_e + \frac{1}{3}W_L n_N,
 \end{aligned} \tag{1}$$

where n_b is the baryon number density and n_N is the number density of nuclei; those two are connected by $n_b = An_N$. The energy of the nucleus (including rest mass energy of nucleons) is

$$W_N = m_n(A - Z) + m_p Z - bA, \quad (2)$$

where b is the binding energy per nucleon. We obtain experimental nuclear masses from the atomic mass table of Ref.([13]). We exploit the theoretical extrapolation for the rest of nuclei [14]. The lattice energy of the cell W_L is given below [15],

$$W_L = -\frac{9}{10} \frac{Z^2 e^2}{r_C} \left(1 - \frac{5}{9} \left(\frac{r_N}{r_C} \right)^2 \right). \quad (3)$$

The cell and nucleus radii are r_C and r_N , respectively. The first term in Eq.(3) is the lattice energy for point nuclei and the second term corresponds to the finite size effect [15].

Now we focus on the impact of strong magnetic fields on the Gibbs free energy per baryon. In presence of a magnetic field, the motion of charged particles perpendicular to the magnetic field is quantised into Landau levels. This is known as Landau Quantisation [16]. In this calculation, we are interested only in Landau quantisation of electrons and its influence on ground state properties of neutron star crusts. The electron energy density (ε_e), pressure (P_e) and number density (n_e) due to Landau quantisation of electrons are given below [12],

$$\begin{aligned} \varepsilon_e &= \frac{eB}{4\pi^2} \sum_{\nu=0}^{\nu_{max}} g_\nu \left(p_{F_{e,\nu}} \mu_e + (m_e^2 + 2eB\nu) \ln \frac{p_{F_{e,\nu}} + \mu_e}{\sqrt{(m_e^2 + 2eB\nu)}} \right), \\ P_e &= \frac{eB}{4\pi^2} \sum_{\nu=0}^{\nu_{max}} g_\nu \left(p_{F_{e,\nu}} \mu_e - (m_e^2 + 2eB\nu) \ln \frac{p_{F_{e,\nu}} + \mu_e}{\sqrt{(m_e^2 + 2eB\nu)}} \right), \\ n_e &= \frac{eB}{2\pi^2} \sum_{\nu=0}^{\nu_{max}} g_\nu p_{F_{e,\nu}}, \end{aligned} \quad (4)$$

where B is the magnetic field, ν_{max} is the maximum Landau quantum number, $p_{F_{e,\nu}} = \sqrt{\mu_e^2 - (m_e^2 + 2\nu eB)}$, μ_e is the electron chemical potential, and the spin degeneracy $g_\nu = 1$ for $\nu = 0$ and $g_\nu = 2$ for other values of Landau quantum numbers. We define $B_* = B/B_c$, where the critical field for electrons is $B_c = 4.414 \times 10^{13}$ G. In the following paragraphs, we use magnetic field strengths in terms of B_* .

Electron number density is greatly influenced due to Landau quantization in strongly quantising magnetic fields. For $B_* \leq 10^3$, electrons populate large number of Landau levels. Consequently, there is no change in electron number density compared with the zero field situation. However, electron number density strongly enhanced when the field is $B \geq 10^{17}$ G. This is attributed to the fact that electrons populate only the zeroth Landau level [12]. This might impact the composition and EoS of the outer crust.

We calculate the sequence of nuclei in the outer crust for $B = 0$ and $B_* = 10^3$. Results are shown in Table 1 and Table 2. A careful examination of results in both tables shows that nucleus such as ^{78}Ni which is present for $B = 0$, is absent in the case of $B_* = 10^3$. Similarly, two new nuclei ^{88}Sr and ^{128}Pd are found to appear in Table 2. The finite size correction to the lattice energy modifies the sequence of nuclei for $B_* = 10^4$. It is to be noted that our results are different from those of Ref.[11] because we have used the recent experimental and theoretical nuclear mass tables in our calculation. One important result of this calculation is the shift of the neutron drip point to higher density in presence of strong magnetic fields. This is evident when we compare ρ_{max} which is the maximum density for the existence of an equilibrium nucleus, in the last row of Table 1 and Table 2.

Table 1. Sequence of nuclei in the outer crust in absence of magnetic fields. Elements with their charges (Z) and neutron numbers (N), maximum mass density (ρ_{max}), electron number density (n_e), electron chemical potential (μ) and Gibbs free energy per nucleon (g) for $B = 0$ are recorded here.

element	Z	N	ρ_{max} (g/cm ³)	n_e (cm ⁻³)	μ_e (MeV)	g (MeV)
⁵⁶ Fe	26	30	8.01×10^6	2.24×10^{30}	0.95	930.60
⁶² Ni	28	34	2.71×10^8	7.38×10^{31}	2.61	931.32
⁶⁴ Ni	28	34	1.33×10^9	3.51×10^{32}	4.34	932.04
⁶⁶ Ni	28	34	1.50×10^9	3.82×10^{32}	4.46	932.09
⁸⁶ Kr	36	50	3.10×10^9	7.80×10^{32}	5.64	932.56
⁸⁴ Se	34	50	1.06×10^{10}	2.58×10^{33}	8.39	933.62
⁸² Ge	32	50	2.79×10^{10}	6.54×10^{33}	11.43	934.75
⁸⁰ Zn	30	50	6.11×10^{10}	1.37×10^{34}	14.63	935.90
⁷⁸ Ni	28	50	9.25×10^{10}	1.99×10^{34}	16.56	936.57
¹²⁶ Ru	44	82	1.29×10^{11}	2.69×10^{34}	18.30	937.12
¹²⁴ Mo	42	82	1.86×10^{11}	3.78×10^{34}	20.50	937.83
¹²² Zr	40	82	2.64×10^{11}	5.18×10^{34}	22.76	938.53
¹²⁰ Sr	38	82	3.77×10^{11}	7.13×10^{34}	25.33	939.31
¹¹⁸ Kr	36	82	4.34×10^{11}	7.91×10^{34}	26.22	939.57

Table 2. Same as Table 1 but for $B_* = 10^3$.

element	Z	N	ρ_{max} (g/cm ³)	n_e (cm ⁻³)	μ_e (MeV)	g (MeV)
⁵⁶ Fe	26	30	4.31×10^9	1.21×10^{33}	0.87	930.46
⁶² Ni	28	34	1.83×10^{10}	4.99×10^{33}	2.94	931.32
⁶⁴ Ni	28	34	2.33×10^{10}	6.14×10^{33}	3.60	931.59
⁸⁸ Sr	38	50	2.59×10^{10}	6.73×10^{34}	3.94	931.72
⁸⁶ Kr	36	50	4.33×10^{10}	1.09×10^{34}	6.35	932.69
⁸⁴ Se	34	50	6.33×10^{10}	1.54×10^{34}	8.97	933.72
⁸² Ge	32	50	8.67×10^{10}	2.04×10^{34}	11.83	934.82
⁸⁰ Zn	30	50	1.13×10^{11}	2.55×10^{34}	14.82	935.93
¹²⁸ Pd	46	82	1.29×10^{11}	2.78×10^{34}	16.15	936.38
¹²⁶ Ru	44	82	1.50×10^{11}	3.15×10^{34}	18.32	937.13
¹²⁴ Mo	42	82	1.72×10^{11}	3.50×10^{34}	20.35	937.82
¹²² Zr	40	82	1.96×10^{11}	3.86×10^{34}	22.45	938.50
¹²⁰ Sr	38	82	4.34×10^{11}	8.22×10^{34}	25.44	939.32
¹¹⁸ Kr	36	82	4.92×10^{11}	8.98×10^{34}	26.27	939.57

Now we discuss the inner crust. Nuclei of the inner crust are not only immersed in a uniform background of electrons but also in coexistence with a neutron gas. Besides charge neutrality, the matter of the inner crust is in β -equilibrium. The ground state properties of the inner crust in zero magnetic field were studied by several groups [17, 18, 19, 20, 21]. The first calculation of the inner crust in presence of strong magnetic fields was investigated in the Thomas-Fermi (TF) model at zero temperature [22]. Nuclei of the inner crust are also arranged in a bcc lattice. The Wigner-Seitz approximation is used in the calculation of the inner crust in presence of strong magnetic fields. Further, each lattice volume is replaced by a spherical cell with one nucleus at the center. Each cell is charge neutral. There is no Coulomb interaction between cells. In this case, the denser phase in a nucleus is in coexistence with the low density phase of neutron gas. This has to be dealt with in a thermodynamically consistent way. The spherical cell in which protons and neutrons reside, does not define a nucleus. We exploit the subtraction procedure of Bonche, Levit and Vautherin (BLV) [23] to remove the gas part from the nucleus plus gas in the cell. In the BLV scheme, the density profiles of the gas part as well as nucleus plus gas are derived self-consistently in the TF formalism. Finally, the difference of two solutions in BLV scheme determines the nucleus [23, 24]. Here electrons are Landau quantised in strong magnetic fields, but protons in the cell are indirectly affected through the charge neutrality.

Our starting point in this calculation of inner crust is the thermodynamical potential (Ω_N) of a nucleus. This is obtained as the difference of the thermodynamical potential in nucleus plus gas (Ω_{NG}) and that of the gas phase (Ω_G). This is given by [23],

$$\Omega_N = \Omega_{NG} - \Omega_G , \quad (5)$$

where the thermodynamic potential is written in terms of free energy (F), chemical potential (μ_i) and number density (n_i) of i -th species,

$$\Omega = F - \sum_{i=n,p} \mu_i n_i . \quad (6)$$

The free energy is a function of average baryon density (n_b) and proton fraction (Y_p) and given below,

$$F(n_b, Y_p) = \int [\varepsilon_N + \varepsilon_c + \varepsilon_e] d\mathbf{r} . \quad (7)$$

The free energy contains nuclear energy density (ε_N), Coulomb energy density (ε_c) and electron energy density. We calculate the nuclear energy density using Skyrme (SkM) nucleon-nucleon interaction [22, 25, 26, 27]. We minimise the thermodynamical potential with respect to baryon density in each phase and obtain neutron and proton density profiles of two phases solving coupled equations [22, 28]. The chemical potential in presence of magnetic fields is [22]

$$\mu_e = \left[p_{F_{e,\nu}}^2 + m_e^2 + 2eB\nu \right]^{1/2} - \langle V^c(r) \rangle , \quad (8)$$

where $\langle V^c(r) \rangle$ denotes the average single particle Coulomb potential. As soon as we know density profiles in two phases, we calculate mass and atomic numbers of a nucleus using the subtraction procedure of BLV [22].

Now we present our results of the inner crust. As electrons are Landau quantised in strong magnetic fields, we show its impact on electron number density. Figure 2 shows electron number density as a function of mass density. For $B_* = 10^3$ or smaller field strength, large numbers of Landau levels are populated by electrons. As a result, the electron number density does not differ from the zero field results. For stronger magnetic fields such as $B_* = 10^4$, electrons populate the zeroth Landau level or a few levels over a certain mass density regime. In this

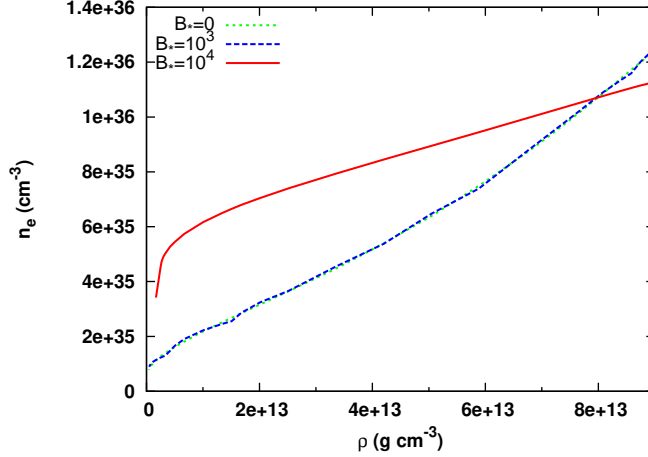


Figure 2. Electron number density is plotted with mass density for different magnetic field strengths.

case, it is evident from Fig. 2 that electron number density is significantly enhanced compared with the zero field case. However, the situation is different at higher densities. We do not see any enhancement of electron fraction there. Proton fraction is modified in presence of strong magnetic fields through charge neutrality. Neutrons are affected by magnetic fields through β -equilibrium. The outcome of this is fewer neutrons drip out of a nucleus in presence of strong magnetic fields [22].

Next we obtain the equilibrium nucleus at each density point by minimising the free energy per particle of the cell [22]. In the left panel of Fig. 3, we show the sequence of equilibrium nuclei and their corresponding free energies per particle as a function of mass density with and without magnetic field. Furthermore, this calculation is done without subtracting the gas part. It is noted that the free energy per nucleon is reduced in strong magnetic fields of $B_* = 10^4$. This is attributed to the population of electrons in the zeroth Landau level. However, free energy per nucleon for $B = 0$ and $B_* = 10^4$ come closer when large number of Landau levels are populated at higher densities. For zero magnetic field case, we find excellent qualitative agreement between our results and those of Negele and Vautherin [20]. In the right panel of Fig. 3, mass and atomic numbers of equilibrium nuclei are shown after applying the subtraction method of BLV. We find that mass and atomic numbers increase in presence of a strong magnetic field compared with the results of zero magnetic field.

We repeat the calculation of inner crust with SLy4 [29] and Sk272 [30] nucleon-nucleon interactions. Results of these calculations are shown in Fig. 4. We find qualitatively similar results for mass and atomic numbers as a function of average baryon number density as found in case of SkM interaction. For SLy4 interaction, we find mass and atomic numbers in the magnetic field jump when electrons in the zeroth Landau level move to the next level around baryon number density $0.05 fm^{-3}$. Further, we note that the SLy4 parameter set results in higher mass and atomic numbers because of stiffer density dependence of the symmetry energy at sub-saturation densities than that of other parameter sets considered here.

3. Torsional Shear Modes

Next we are interested in the role of compositions and EoS of magnetised crusts that we have described in section 2, on torsional shear modes of magnetars. It is argued that torsional shear

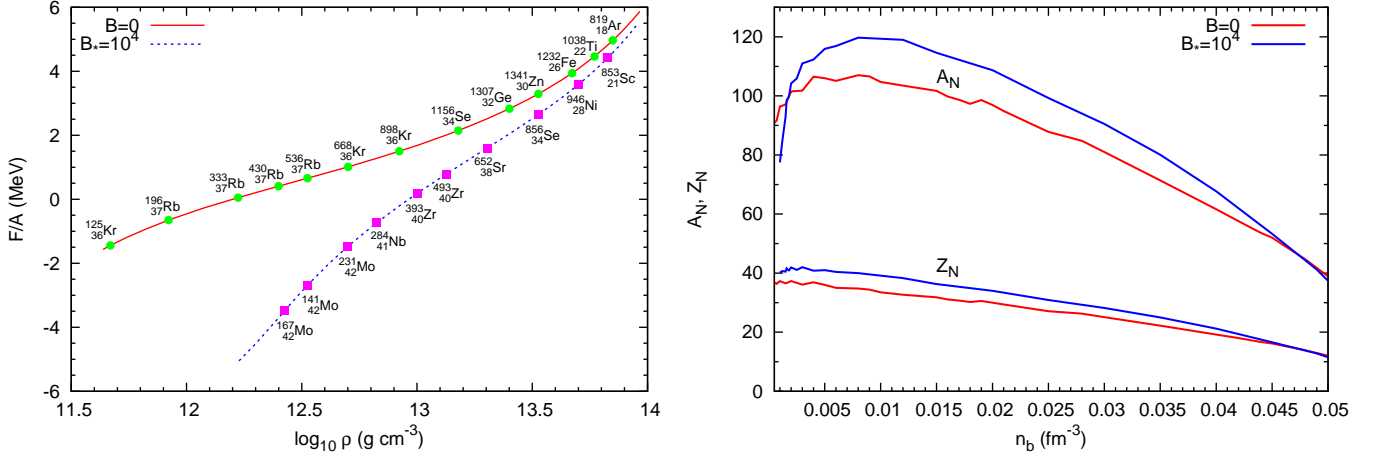


Figure 3. Free energy per nucleon of the cell is plotted with mass density for zero magnetic field, $B = 10^3$ and $B_* = 10^4$ (left panel). Equilibrium nuclei are denoted with solid symbols in both panels; mass and atomic numbers in nuclei after the subtraction of the gas phase is shown as a function of average baryon number density (left panel).

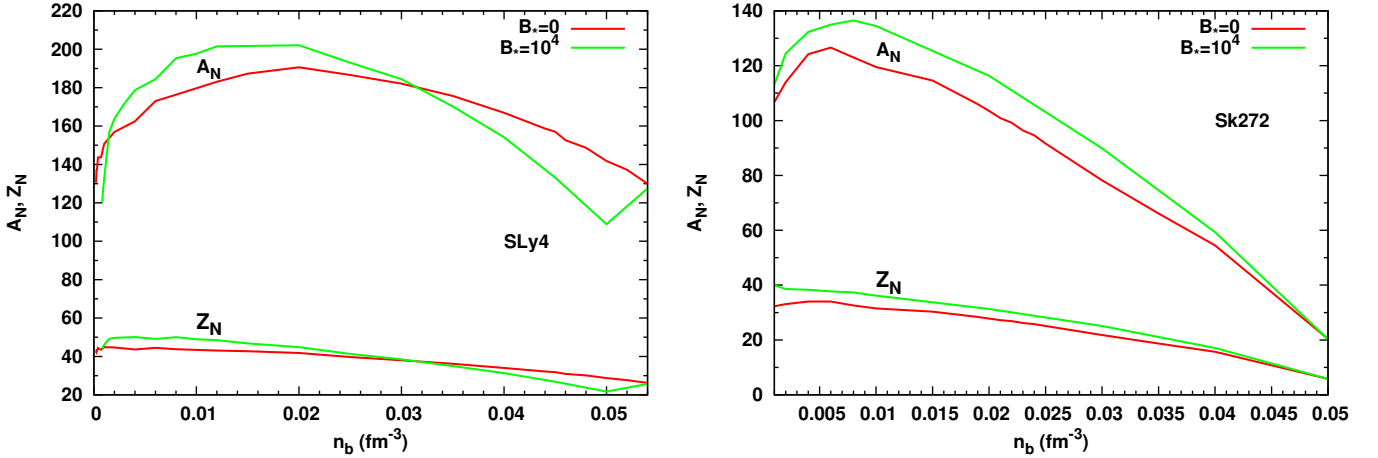


Figure 4. Mass and atomic numbers in nuclei after the subtraction of the gas phase is shown as a function of average baryon number density for SLy4 interaction (left panel) as well as Sk272 (right panel) with $B = 0$ and $B_* = 10^4$.

mode frequencies depends on the shear modulus of neutron star crusts [8, 9, 31]. Further the shear modulus is sensitive to compositions and EoS of neutron star crusts. This implies that nuclear physics plays an important role in determining torsional shear frequencies [31]. Here we describe the calculation of the shear modulus and shear velocity of the magnetised neutron star crusts. We use the following the expression of the shear modulus (μ) at zero temperature [32, 33],

$$\mu = 0.1194 \frac{n_i (Ze)^2}{a}, \quad (9)$$

where $a = 3/(4\pi n_i)$, Z is the atomic number of a nucleus and n_i is the ion density. This form of the shear modulus was obtained by assuming a bcc lattice and performing directional averages

[34]. We exploit inputs n_i and a from the magnetised crusts of section 2. We immediately calculate the shear speed as $v_s = \sqrt{(\mu/\rho)}$. In Figure 5, the shear speed is shown as a function of mass density with and without magnetic field. For $B_* = 10^3$, the shear speed does not differ from that of $B = 0$. In presence of strong fields such as $B_* = 10^4$, the shear speed enhanced compared with the zero field results. We find spikes in each curve. It happens when an equilibrium nucleus jumps to a new one in the outer crust.

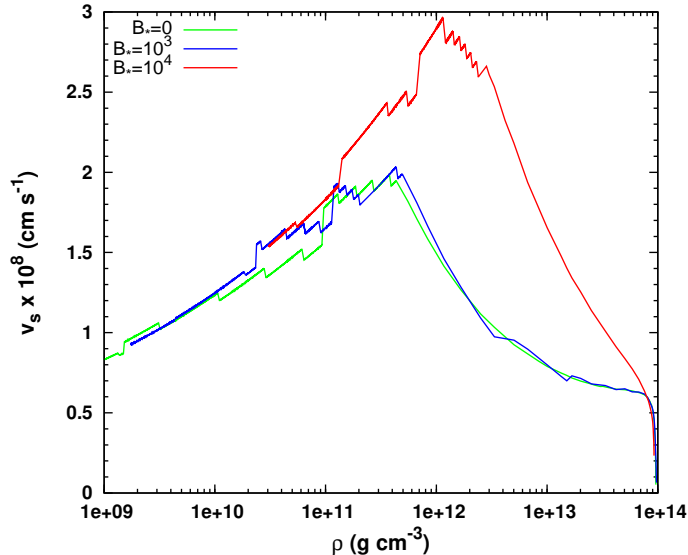


Figure 5. Shear velocity is shown as a function of mass density for different magnetic field strengths.

Torsional shear modes were studied extensively using non-magnetic crusts in Newtonian gravity [3, 35, 36, 37] and general relativity [38, 39, 40, 41, 42]. Here we are interested in the effects of magnetised crusts on torsional shear mode frequencies. We adopt the model of Refs.[38, 42] to calculate torsional shear frequencies in presence of a dipole magnetic field. In this calculation, we consider the magnetised crust decoupled from the core. Further, the magnetised star is considered to be the spherically symmetric because the deformation due to the magnetic field is neglected [42]. The perturbed equations describing torsional shear modes are obtained by linearising the equations that govern equilibrium configurations. Equilibrium stellar models are determined using the metric

$$ds^2 = -e^{2\Phi} dt^2 + e^{2\Lambda} dr^2 + r^2 (d\theta^2 + \sin^2\theta d\phi^2) . \quad (10)$$

We consider axial-type perturbation in the four velocity (u^μ) and the only non-vanishing perturbed quantity is the ϕ component of the perturbed four velocity u^ϕ [38]

$$\partial u^\phi = e^{-\phi} \partial_t \mathcal{Y}(t, r) \frac{1}{\sin\theta} \partial_\theta P_\ell(\cos\theta) , \quad (11)$$

where ∂_t and ∂_θ correspond to partial derivatives with respect to time and θ , respectively, $P_\ell(\cos\theta)$ is the Legendre polynomial of order ℓ and $\mathcal{Y}(t, r)$ is the angular displacement of the matter. Assuming a harmonic time dependence of $\mathcal{Y}(t, r)$, one arrives at the eigenvalue equation which is a second order differential equation [38]. Finally, we estimate eigenfrequencies by solving

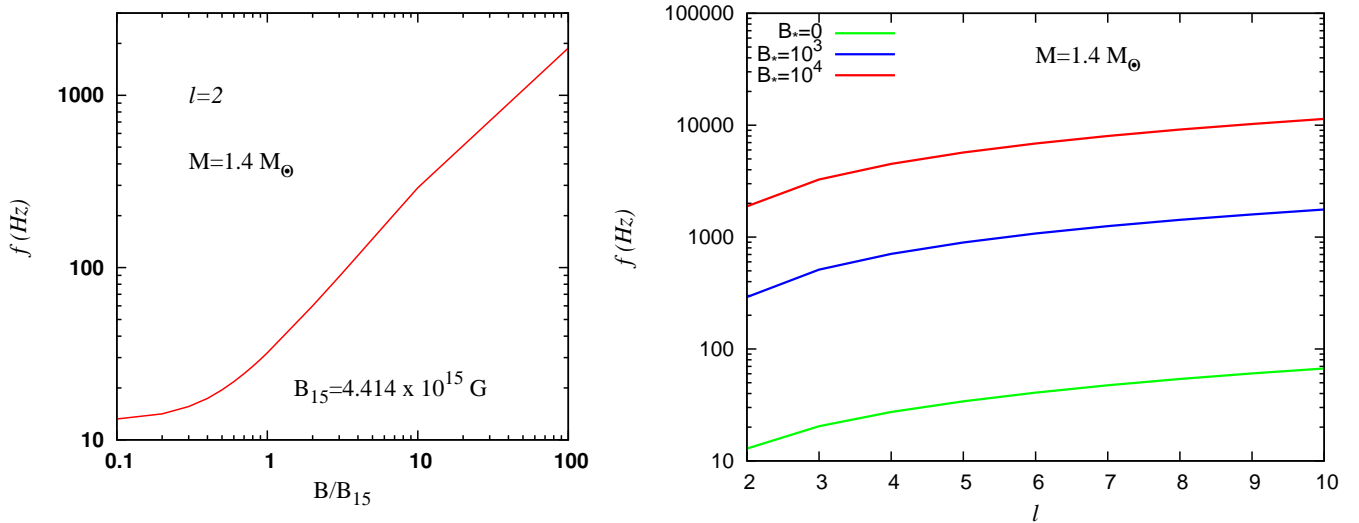


Figure 6. Fundamental ($n = 0$, $\ell = 2$) shear mode frequency as a function of normalised magnetic field for a neutron star of $1.4 M_{\odot}$ (left panel); Torsional shear mode frequency ($n = 0$) as a function of ℓ values for different magnetic field strengths and a neutron star of $1.4 M_{\odot}$ (right panel).

two first order differential equations Eq.(69) and (70) of Sotani et al. with appropriate boundary conditions [38].

Now we discuss the results of our calculation using the magnetised crusts calculated with SkM nucleon-nucleon interaction. In the left panel of Figure 6, fundamental shear mode frequency ($n = 0$, $\ell = 2$) is plotted with magnetic field for a neutron star of $1.4 M_{\odot}$. The fundamental frequency increases with increasing magnetic field. This plot implies if we know the mass of the star and the field strength accurately, we can determine the frequency and compare it with the observed frequency. In the right panel of Figure 6, we show torsional shear mode frequency for $n = 0$ as a function of ℓ values. As ℓ values increase, the frequency increases. It is also evident from this figure that the torsional frequency increases with increasing magnetic field strengths. It is also noted that frequencies of torsional shear modes decrease with increasing masses of magnetars [43].

Finally, we calculate fundamental torsional shear mode frequencies as well as various overtones for SGR 1806-20 and SGR 1900+14 and compare those with observed frequencies of QPOs. We show this comparison in Table 3 and Table 4. In case of SGR 1806-20, higher torsional frequencies i.e. (93, 150, 626 and 1838 Hz) are nicely explained by our theoretical calculation with magnetised crusts when the magnetic field is $B = 8 \times 10^{14}$ G and mass is $1.4 M_{\odot}$ [43]. However, the agreement of three lower frequencies (18, 26 and 29 Hz) with our calculation is not good. These frequencies could possibly be explained by the Alfvén modes [44]. On the other hand, all four observed frequencies (28, 55, 82, 154 Hz) in SGR 1900+14 are in excellent agreement with our calculation when the mass is $1.2 M_{\odot}$ and magnetic field $B = 4 \times 10^{14}$ G [43].

4. Summary

We have developed a model of magnetised neutron star crusts. In this context, we have investigated the effects of Landau quantisation of electrons on the ground state properties of outer and inner crusts. It is observed that composition and EoS of neutron star crusts

Table 3. Calculated torsional shear mode frequencies are compared with observed frequencies of SGR 1806-20.

SGR 1806-20			
Observed Frequency (Hz)	Calculated Frequency (Hz)	n	ℓ
18	15	0	2
26	24	0	3
29	32	0	4
93	93	0	12
150	151	0	20
626	626	1	29
1838	1834	4	2

Table 4. Same as Table 3 but for SGR 1900+14.

SGR 1900+14			
Observed Frequency (Hz)	Calculated Frequency (Hz)	n	ℓ
28	28	0	4
54	55	0	8
84	82	0	12
155	154	0	23

are appreciably modified in strong magnetic fields. We have calculated the shear modulus and shear velocity in connection with torsional shear modes. It is found that torsional shear frequencies calculated using our model of magnetised crusts are in good agreement with the observed frequencies of QPOs.

5. Reference

- [1] Yakovlev D G and Kaminker A D The Equation of State in Astrophysics Chabrier G and Schatzman E, ed., (Cambridge University Press, Cambridge, 1994) p214
- [2] Duncan R C and Thompson C 1992 *Astrophys. J.* **392** L9
- [3] Duncan R C 1998 *Astrophys. J.* **498** L45
- [4] Kouveluotou C et al. 1998 *Nature* **393** 235
- [5] Kouveluotou C et al. 1999 *Astrophys. J.* **510** L115
- [6] Barat C et al. 2003 *Astron. Astrophys.* **126** 400
- [7] Israel G L et al. 2005 *Astrophys. J.* **628** L53
- [8] Watts A L 2011 *arXiv:1111.0514*
- [9] Watts A L and Strohmayer T E 2007 *Advances in Space Research* **40** 1446
- [10] Baym G, Pethick C and Sutherland P 1971 *Astrophys. J.* **170** 299
- [11] Lai D and Shapiro S L 1991 *Astrophys. J.* **383** 745
- [12] Nandi R and Bandyopadhyay D 2011 *J. Phys. Conf. Ser.* **312** 042016
- [13] Audi G, Wapstra A H and Thibault C 2003 *Nucl. Phys. A* **729** 337
- [14] Moller P, Nix J R, Myers W D and Swiatecki W J 1995 *At. Data Nucl. Data Tables* **59** 185
- [15] Baym G, Bethe H A and Pethick C J 1971 *Nucl. Phys. A* **175** 225
- [16] Lai D 2001 *Rev. Mod. Phys.* **73** 629
- [17] W Langer D, Rosen L C, Cohen J M and A G W Cameron A G W 1969 *Astrophys. Space. Sc.* **5** 529
- [18] Bethe H A, Borner G and Sato K 1970 *Astron. Astrophys.* **7** 270
- [19] Baym G, Bethe H A, and Pethick C J 1971 *Nucl. Phys. A* **175** 225
- [20] Negele J W and Vautherin D 1973 *Nucl. Phys. A* **207** 298
- [21] Cheng K S, Yao C C and Dai Z C 1997 *Phys. Rev. C* **55** 2092
- [22] Nandi R, Bandyopadhyay D, Mishustin I N and Greiner W 2011 *Astrophys. J.* **736** 156
- [23] Bonche P, Levit S and Vautherin D 1984 *Nucl. Phys. A* **427** 278; Bonche P, Levit S and Vautherin D 1985 *Nucl. Phys. A* **436** 265
- [24] Suraud E 1987 *Nucl. Phys. A* **462** 109
- [25] Krivine H, Treiner J and Bohigas O 1980 *Nucl. Phys. A* **336** 115
- [26] Brack M, Guet C and Håkansson H B 1985 *Phys. Rep.* **123** 275
- [27] Stone J R, Miller J C, Koncewicz R, Stevenson P D and Strayer M R 2003 *Phys. Rev. C* **C68** 034324
- [28] Sil T et al. 2002 *Phys. Rev. C* **66** 045803
- [29] Chabanat E et al. 1998 *Nucl. Phys. A* **635** 231
- [30] Agrawal B K, Shlomo S and Au V Kim 2003 *Phys. Rev. C* **68** 031304
- [31] Steiner A W and Watts A L 2009 *Phys. Rev. Lett.* **103** 181101
- [32] Ogata S and Ichimaru S 1990 *Phys. Rev.* **A42** 4867
- [33] Strohmayer T, van Horn H M, Ogata S, Iyetomi H and Ichimaru S 1991 *Astrophys. J.* **375** 679
- [34] P. Haensel, in Neutron Star crusts ed. Blaschke D, Glendenning N K and Sedrakian A Lecture Notes in Physics: Physics of Neutron Star Interiors, (Springer, Heidelberg), vol 578, p127
- [35] Piro A L 2005 *Astrophys. J.* **634**, L153
- [36] Carrol B W et al. 1986 *Astrophys. J.* **305** 767
- [37] McDermott P N, van Horn H M and Hansen C J 1988 *Astrophys. J.* **325** 725
- [38] Sotani H, Kokkotas K D and Stergioulas N 2007 *Mon. Not. R. Astron. Soc.* **375** 261
- [39] Sotani H, Kokkotas K D and Stergioulas N 2008 *Mon. Not. R. Astron. Soc.* **385** L5
- [40] Sotani H 2011 *Mon. Not. Astron. Soc.* **417** L70
- [41] Schumaker B L and Thorne K S 1983 *Mon. Not. R. Astron. Soc.* **203** 457
- [42] Messios N, Papadopolous D B and Stergioulas N 2001 *Mon. Not. R. Astron. Soc.* **328** 1161
- [43] Nandi R, Chatterjee D and Bandyopadhyay D 2012 *arXiv:1207.3247*
- [44] Colaiuda A and Kokkotas K D 2011 *Mon. Not. R. Astron. Soc.* **414** 3014